Journal of Hydrology 574 (2019) 75–84

Contents lists available at ScienceDirect

Journal of Hydrology

journal homepage: www.elsevier.com/locate/jhydrol

Research papers

Influences of riverbed morphology on patterns and magnitudes of hyporheic water exchange within a natural river confluence

Dandong Cheng[a,b], Jinxi Song[a,c,*], Weize Wang[d,e], Guotao Zhang[b,f]

[a] State Key Laboratory of Soil Erosion and Dryland Farming on the Loess Plateau, Institute of Soil and Water Conservation, Chinese Academy of Sciences and Ministry of Water Resources, Yangling, Shaanxi 712100, China
[b] University of Chinese Academy of Sciences, Beijing 100049, China
[c] Shaanxi Key Laboratory of Earth Surface System and Environmental Carrying Capacity, College of Urban and Environmental Sciences, Northwest University, Xi'an 710127, China
[d] State Key Laboratory of Simulation and Regulation of Water Cycle in River Basin, China Institute of Water Resources and Hydropower Research, Beijing 100038, China
[e] Department of Hydraulic Engineering, Tsinghua University, Beijing 100084, China
[f] Key Laboratory of Mountain Hazards and Earth Surface Process, Institute of Mountain Hazards and Environment, Chinese Academy of Sciences, Chengdu 610041, China

ARTICLE INFO

Keywords:
River confluence
Morphology
Hydraulic characteristics
Sedimentary properties
Hyporheic water exchange

ABSTRACT

River confluences are pivotal junctions that have vital influences on hydraulic characteristics and sediment particle distributions as well as on hyporheic water exchange. However, hyporheic water exchange is poorly understood because of the complicated river morphology within a river confluence. Therefore, the river confluence between the Juehe River and Haohe River located in arid and semi-arid areas of northwestern China was selected to evaluate the hyporheic water exchange processes, and the temperatures of different depth sediment were measured on July 11th and 12th, 2016 by an instrument equipped with five temperature sensors. The patterns and magnitudes of hyporheic water exchange were estimated using a one-dimensional heat transport model coupled with temperature data. Meanwhile, terrain points elevations and sediment particle distributions in this river confluence were collected to determine the confluence riverbed morphology. Furthermore, the river confluence morphology effects on hyporheic water exchange were investigated in this study. The different riverbed morphology and hydrodynamic zone locations were observed, which were controlled by the planform geometry with low river confluence flux momentum during the test period. Meanwhile, the upwelling flow dominated in the test area, and the downwelling occurred at three of the 23 total test points, which was induced by the complicated riverbed morphology and hydraulic characteristics. Additionally, the magnitudes of the upwelling flow were significantly influenced by the sediment heterogeneity subjected to the erosional and depositional processes. Hyporheic water exchange is a vital hydrological process in arid and semi-arid areas, where it significantly impacts the ecological environment of rivers. This study provides a valuable guideline for water quality and quantity management in arid and semi-arid areas.

1. Introduction

Rivers are a typical geomorphic feature on the Earth's land surface with a variety of environmental and service functions. Surface water and groundwater are not independent hydrological systems (Boulton et al., 1998; Chen et al., 2017b). Surface–groundwater exchange commonly occurs in the hyporheic zone of rivers (Jones and Holmes, 1996). The hyporheic zone is the sediment layer within the riverbed that is saturated with water and is located in the intermediate zone between surface water and groundwater, which is the zone that connects rivers and groundwater systems (Boulton et al., 1998; Zarnetske et al., 2012; Cranswick et al., 2014). Hyporheic water exchange drives the physical, chemical and biological characteristics of the hyporheic zone, controls interaction between the surface water and groundwater (Brunke and Gonser, 1997), and further, influences the quality and quantity of surface water and groundwater (Kalbus et al., 2007; Chen et al., 2018). Meanwhile, the hyporheic zone is regarded as the liver of the river due to biodegradation and adsorption of pollutants within river systems (Storey et al., 2004; Fischer et al., 2005; Briggs et al., 2014). Hence, research on hyporheic water exchange has gradually attracted the

* Corresponding author at: Shaanxi Key Laboratory of Earth Surface System and Environmental Carrying Capacity, College of Urban and Environmental Sciences, Northwest University, Xi'an 710127, China.
E-mail address: jinxisong@nwu.edu.cn (J. Song).

https://doi.org/10.1016/j.jhydrol.2019.04.025

Available online 06 April 2019

attention of researchers and has become vital in international studies (Krause et al., 2009). Furthermore, in arid and semi-arid regions, hyporheic water exchange is an extremely important hydrologic process that has significant effects on the water quality and quantity of rivers due to the reduced precipitation rainfall capacity (Wang et al., 2008, 2013; Chen et al., 2017a).

The accurate estimation of hyporheic water exchange patterns and magnitudes is an essential task in the research of water exchange. In previous studies, many methods were used to determine the patterns and magnitudes of hyporheic water exchange, including tracer tests (Yang et al., 2012), the Darcy equation (Anderson, 2005), thermal methods (Hatch et al., 2006), seepage meters (Zhu et al., 2015) and other methods (Wei et al., 2011; Zhang et al., 2017). However, different measurement scales and hydrogeological conditions limit the application of these methods in field studies. For example, tracer tests and baseflow separation determine ground-surface water exchange at the catchment scale (Hatch et al., 2006) and a seepage meter is generally used to assess riverbed seepage within relatively smooth riverbeds (Zhu et al.,2015). Heat has been increasingly used to estimate the hyporheic water exchange patterns and magnitudes because heat is a valid, natural tracer that can be used on multiple scales (Anderson, 2005; Hatch et al., 2006). Remarkably, collecting and measuring temperature data in the hyporheic zone is simple and convenient in many field studies. Stallman (1965) developed a one-dimensional heat transport model that estimated hyporheic water exchange processes based on the theory that hyporheic water flow occurs simultaneously with heat transfer. Bredehoeft and Papaopulos (1965) proposed a one-dimensional steady-state heat model based on the steady-state thermal assumption. Furthermore, the model was developed by Anibas et al., (2009) to evaluate the hyporheic water exchange patterns and magnitudes on various stream topographies. Engelhardt et al (2011) collected temperature data to study groundwater-surface water interactions in Schwarzbach, Germany by the model. Wang et al (2018) measured riverbed temperatures and sampled riverbed sediment in the Weihe River to estimate hyporheic water exchange and further analyze the effect of water exchange on inorganic nitrogen within pore water.

The topography of the river bank or riverbed has a significant influence on hyporheic water exchange (Kasahara and Wondzell, 2003). Hill et al. (1998) found that changes in longitudinal gradients in-stream channel riffle-pool units induced small-scale vertical and horizontal hyporheic water exchanges. Meanwhile, Boano et al. (2006) indicated that the process of surface-groundwater exchange in river bends is more significant relative to that in straight channels. However, deposition and erosion caused by flow along river bends also influences the hyporheic flow through river sediment (Song et al., 2016; Zhang et al., 2016). Gravel bars are also a common topographic feature in a natural channel. Wondzell and Swanson (1999) found that while lateral flow typically dominates gravel bars, a large flood event created extensive hyporheic zones with increased downward flux at the head of several gravel bars while lateral downstream river-bar interactions were maintained. Thus, the patterns and magnitudes of hyporheic water exchange are easily induced by the river bank topography or riverbed forms such as riffle-pools, gravel bars and river bends (Boano et al., 2006; Shope et al., 2012; Stonedahl et al., 2013). However, the vast majority of studies have focused on the effects of relatively large geomorphological structures on hyporheic water exchange (Wondzell and Swanson, 1999; Stonedahl et al., 2013). Under complex river topographic conditions, small-scale variability in hyporheic water exchange affected by river morphology at a river confluence is still not fully understood. Therefore, estimating hyporheic water exchange and analyzing the influences of riverbed morphology on patterns and magnitudes of hyporheic water exchange not only provide a useful clue to understanding the hydrological processes but also provide a vital guide for the management of water quantity and quality in arid and semi-arid regions.

A river confluence is an important morphological element in the river system. The morphology of the river confluence commonly consists of an avalanche face, confluence scour, and separation zone bar (Best, 1988). The avalanche face produced by severe flow deflection, rapid growth rate and shear stress when the two streams entered the confluence is more pronounced at higher confluence angles. Confluence scour refers to the scouring ditch formed by the increase in velocity and turbulence level at the junction when the two streams merge. The separation zone bar is located at the corner of the lower reaches, which is formed by the lower fluid velocity and pressure when the sediment from the tributaries is involved in the separation area (Best, 1986; Best and Rhoads, 2008). All of these features of flow dynamics and sediment transport within the river confluence, such as erosion and deposition processes, are induced by the river confluence morphology (Boano et al., 2006). Furthermore, the characteristics of flow dynamics and grain size distributions (including silt-clay as well as median grain size [d50]) significantly influence the hyporheic water exchange patterns and magnitudes (Song et al., 2016). In this study, the river confluence between Juehe River and Haohe River located in the arid and semi-arid areas of Northwestern China was selected to evaluate the hyporheic water exchange processes, and the temperatures data of different sediment layers were measured on July 11 and 12, 2016 and used to quantitatively estimate the patterns and magnitudes of hyporheic water exchange using the one-dimensional steady-state heat transport model. Meanwhile, the river confluence morphology was measured and sediment was sampled in the field study. The particle size of the sediment was analyzed in the laboratory. The objectives of this study are to (1) investigate the morphological features of a river confluence, (2) estimate the spatial variability of the magnitudes and patterns of hyporheic water exchange, and (3) further explore the effects of river morphology and sediment grain size distribution on hyporheic water exchange in the test area.

2. Study area

The study was conducted in the confluence of the Juehe River (main channel) and Haohe River (tributary channel) and was performed in Xi'an City, Shaanxi Province, China on July 11 and 12, 2016. The Juehe River is a secondary tributary of the Weihe River in the Guanzhong Plain. The Juehe River total length and drainage area are 64.2 km and 687 km^2, respectively. The Haohe River has a total length of 46 km and a drainage area of 292 km^2. The Haohe River flows into the Juehe River near the Xiangji Temple in the southern portion of Xi'an city. The two streams both originate from the Tsinling Mountains and finally flow into the Weihe River.

The Juehe River Basin is located in an arid and semiarid climate zone with an average annual rainfall of approximately 660 mm (Guo et al., 2018). The weather in the Juehe River Basin is hot and rainy in summer and cold and dry in winter (Song et al., 2015). Similar to most rivers in arid and semi-arid areas, Juehe River presents active interactions between surface water and groundwater that significantly impact the heavy metal and nitrogen concentration of surface water and groundwater (Liu et al., 2017; Guo et al., 2018). In addition, the Juehe and Haohe Rivers, both located in the southern Weihe River Basin and near the Tsinling Mountains, contain bed materials largely composed of coarse sand, gravel, and even cobbles, which easily induces significant hyporheic water exchange. Meanwhile, the two rivers are crucial for human health and economic consumption on the Guanzhong Plain in Shaanxi Province which includes Xi'an City (Zhi et al., 2013).

The test site is located in the confluence of the Juehe and Haohe Rivers, which is in the southern portion of Xi'an City (Fig. 1a). Field measurements were conducted, and a total of 23 test points were established in the confluence (Fig. 1b). Nine test points were established in the tributary channel (T), five test points were established in the main channel (M), and another nine test points were established in the postconfluence main channel (PM). Each transect included 2 or 3 test points with 10–15 m spacing based on morphological features observed

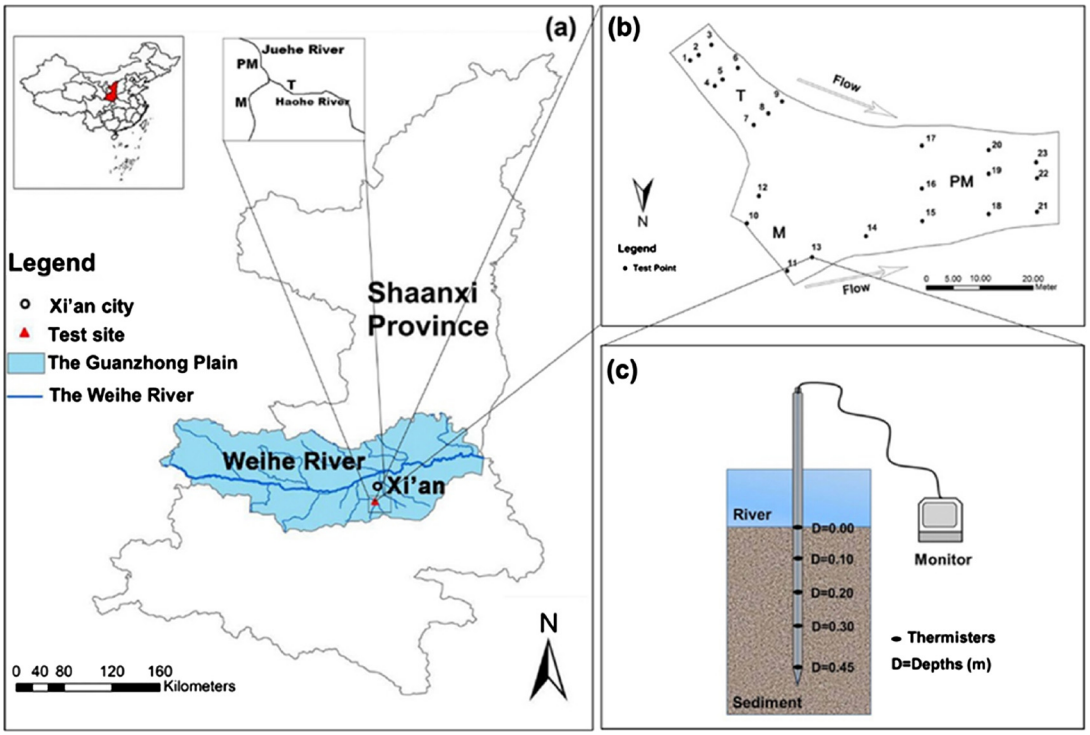

Fig. 1. (a) Map of the study area showing the location of the test site, (b) the test points in the test area, and (c) a schematic diagram of the equipment used for temperature measurements in the streambed sediments.

during field measurements. In addition, no test point was established in the center of the confluence due to equipment length limitations. From July 9 to 13, 2016, rainfall events did not occur, and the groundwater level and river level were stabilized in test area, which was important for avoiding the influence of climatic conditions on hyporheic water exchange.

3. Method

3.1. Sediment temperature measurements

During the test period, temperature data of specific depth sediment layers at the 23 test points were collected by a 2.0 m instrument equipped with 5 temperature sensors at specific depths (0.0 m, 0.1 m, 0.2 m, 0.3 m and 0.45 m) (Fig. 1c). The lower part of the instrument was marked with a length scale to insert the instrument into the sediment at a depth of 0.45 m. Five temperature sensors were used to collect specific depth sediment layer temperature data. The temperature sensors in different sediment layers began working after the instrument was inserted into the river sediment. A measurement required approximately 30 min for the temperature sensors to reach thermal steady-state conditions. The instrument also consists of a data logger that can continuously record and store temperature data of the five sensors (Fig. 1c). The instrument with an accuracy of ± 0.05 °C was calibrated to obtain accurate temperature data after each measurement. Then, the measured temperature data and other physical parameters were input to a one-dimensional heat transport model provided by Bredehoeft and Papaopulos (1965) to obtain the hyporheic water exchange patterns and magnitudes.

3.2. One-dimensional heat transport model

Heat is a vital natural tracer in the determination of hyporheic water exchange patterns and magnitudes (Anibas et al., 2009). Stallman (1965) developed the following equation to estimated patterns and magnitudes of hyporheic water exchange under the assumption that river sediment is isotropic, homogeneous and saturated.

$$\frac{\partial^2 T}{\partial x^2} + \frac{\partial^2 T}{\partial y^2} + \frac{\partial^2 T}{\partial z^2} - \frac{c_f \rho_f}{k}\left[\frac{\partial (v_x T)}{\partial x} + \frac{\partial (v_y T)}{\partial y} + \frac{\partial (v_z T)}{\partial z}\right] = \frac{c_{fs}\rho_{fs}}{k}\frac{\partial T}{\partial t} \quad (1)$$

where

T-temperature at time t
c_f-specific heat of fluid
ρ_f-density of fluid
c_{fs}-specific heat of solid-fluid complex
ρ_{fs}-density of solid-fluid complex
k-thermal conductivity of solid-fluid complex
v_x,v_y, v_z-components of fluid velocity in the x, y, and z directions
x, y, z-Cartesian coordinates
t – time

The expressionv_x,v_y = 0 is based on the assumption that hyporheic water exchange is one-dimensional (in the vertical direction), and thus, Eq. (1) can be simplified to Eq. (2):

$$c_{fs}\rho_{fs}\left(\frac{\partial T}{\partial t}\right) = k_{fs}\frac{\partial^2 T}{\partial z^2} - c_f \rho_f q\left(\frac{\partial T}{\partial z}\right) \quad (2)$$

Bredehoeft and Papaopulos (1965) found that the temperature variations in different sediment layers were very small over time by evaluating the anisothermal groundwater flow through a semi-confining layer in the river. Therefore, an analytical solution was derived in an aquifer system of thickness L (Arriaga and Leap, 2006):

$$T = T_0 \quad z = 0 \quad (3)$$

$$T = T_L \quad z = L \quad (4)$$

Thus, the general differential Eq. (2) was simplified to Eq. (5):

$$\frac{T - T_0}{T_L - T_0} = \frac{e^{\beta(z/L)} - 1}{e^{\beta} - 1} \quad (5)$$

$$\beta = \frac{c_f \rho_f q L}{k_{fs}} \tag{6}$$

where

T-temperature at any depth

T_0-measured uppermost temperature

T_L-measured lowermost temperature

L-vertical distance between measured uppermost and lowermost temperatures

β is a dimensionless parameter, and a positive or negative value of β is determined by the downward or upward value of q, respectively.$\beta = 0$ indicates no vertical flow in the hyporheic zone. A computer program developed by Boyle and Saleem (1979) was used to obtain the sum of deviations between the left and right sides of Eq. (5). The sum of deviation F(β) is as follows:

$$F(\beta) = \sum_{z=0}^{z=L} \left[\frac{T - T_0}{T_L - T_0} - \frac{e^{(\beta z/L)} - 1}{e^{\beta} - 1} \right]^2 \tag{7}$$

The temperatures of the five sediment layers were inputted into Eq. (7) to obtain the optimum value of β when the value of the sum of deviation was minimized. In addition, the downwelling or upwelling fluxes can be obtained by the one-dimensional heat transport model (Eq. (8)). The physical parameters that are inputted into Eq. (8) are shown in Table 1.

$$q = \frac{k_{fs}\beta}{c_f \rho_f L} \tag{8}$$

Positive or negative value of q indicates downwelling and upwelling, respectively, and the value of q indicates magnitudes of hyporheic water exchange.

3.3. Sediment sampling and particle size analysis

At each test point, a 160 cm PVC pipe was inserted into the riverbed next to the temperature pipe. The length of a pipe at the sediment-water interface was approximately 45 cm to obtain 45 cm sediment samples. The top of the pipe was plugged before pulling out the PVC pipe from the riverbed to isolate the interior of the PVC pipe from the atmosphere. Then, the sediment sample that was removed from the PVC pipe was placed into a sampling bag for particle size analysis. Moreover, the sediment samples were air-dried in the laboratory, and the air-dried sediment samples were categorized into 15 grades based on particle sizes using an automatic sieving machine. The largest sieve size was 5 mm, and the smallest sieve size was 0.075 mm. The median grain size (d50) that denotes effective sediment particle size diameter at 50% cumulative weight percentage of particle size was determined by the grain size cumulative curves of each test points. Meanwhile, the grain size can be classified into three groups: gravel (grain size > 2.0 mm), sand (0.075 mm < grain size < 2.0 mm), and silt-clay (grain size < 0.075 mm) (Song et al., 2016).

Table 1
Input parameters of the physical properties for the one-dimensional heat transport equation (Eq. (8)) in the study area.

Parameters	Value	Unit
Thermal conductivity, k_{fs}	1.765*	J s^{-1} m^{-1} K^{-1}
Specific heat capacity of water, c_f	422,400	J kg^{-1} K^{-1}
Density of water, ρ_f	1000	kg m^{-3}
Vertical distance, L	0.45	m

* The value had been defined in a previous study Wang et al. (2018).

3.4. Riverbed topography and surface water and groundwater level measurements

The locations and elevations of terrain points were measured by GPS-RTK (Global Positioning System-Real Time Kinematic) technology using a Trimble R8 mobile receiver (manufactured by American Trimble). A digital elevation model of the river confluence was constructed in ArcGIS, using a Kriging interpolation algorithm. The obtuse junction angle at the river confluence was measured by the average thalweg path along the branches. Meanwhile, the groundwater and surface water level data in the test area from 9 to 13 July 2016 (the groundwater level obtained in a monitoring well situated 200 m off the test area as well as the surface water level at the test site) was monitored every day by the same equipment.

4. Results

4.1. Riverbed morphological characteristics and sediment particle distributions

The planform geometry of the river confluence was Y-shaped with a branch into a meandering channel (Fig. 2a). In the test area, the avalanche faces were observed at the mouths of the two channels, and the scour hole in the central zone near the avalanche face, where the two flows mixed, extended to a depth of approximately 1.5 m (approximately three times the upstream average channel depths). (Fig. 2b). An in-stream gravel bar with a large sediment grain size was observed in the center of the postconfluence channel in the nearby zone of point 19PM (19PM indicates point 19 in PM channel) (Fig. 2b). The greater water depth and thalweg path occurred in the zone near the left bank of the T channel. In the downstream of the river confluence (the PM channel), the topography condition was relatively complex due to the mixing of two flows. In the cross section (including point 15PM, 16PM, and 17PM) and the cross section (including point 18PM, 19PM, and 20PM), the thalweg path nears the left bank because of a flux momentum ratio < 0.5 and the thalweg path in the center zone of the last cross section along the flow direction in the PM (Fig. 2a).

In addition to evaluating the features of the riverbed morphology, the depositional and erosional conditions were also observed in the field study. In the test area, the erosional zones located near the thalweg path were observed in the left bank of the T channel and the center of the downstream channel with less average cumulative percentages by clay weight (0.53% and 1.03%, respectively) (Table 2). Particle size data were not obtained within the center of the M channel due to the limitation of water depth and equipment. However, the sediment particle size distributions indicated that the right and left banks of the M channel were depositional zones. Within the confluence, both sides of the M channel had a higher average cumulative weight percentage of clay or silt and a lower value of d50 than the other channels (the average cumulative weight percentages of clay or silt were 19.56% and 15.46% in the right and left banks of the M channel, respectively) (Table 2).

4.2. General hydraulic characteristics

The main hydraulic parameters were obtained in the field study during the test period (Table 3). The mean flow velocity of the M channel was the largest (mean flow velocity is 2.04 m/s) within the river confluence compared to that in the T and PM channels. Meanwhile, the greatest flow velocity was also observed in the M channel (Table 3). The mean flow velocities of the T and PM channels were 1.48 m/s and 1.03 m/s, respectively (Table 3). The flow dynamics based on the velocities and directions as well as the riverbed topography are shown in Fig. 3. The sites of helicoidal arrows indicate the locations of helicoidal flow cells formed by the confluence of two rivers (Fig. 3). Meanwhile, the riverbed topography was also controlled by the flow

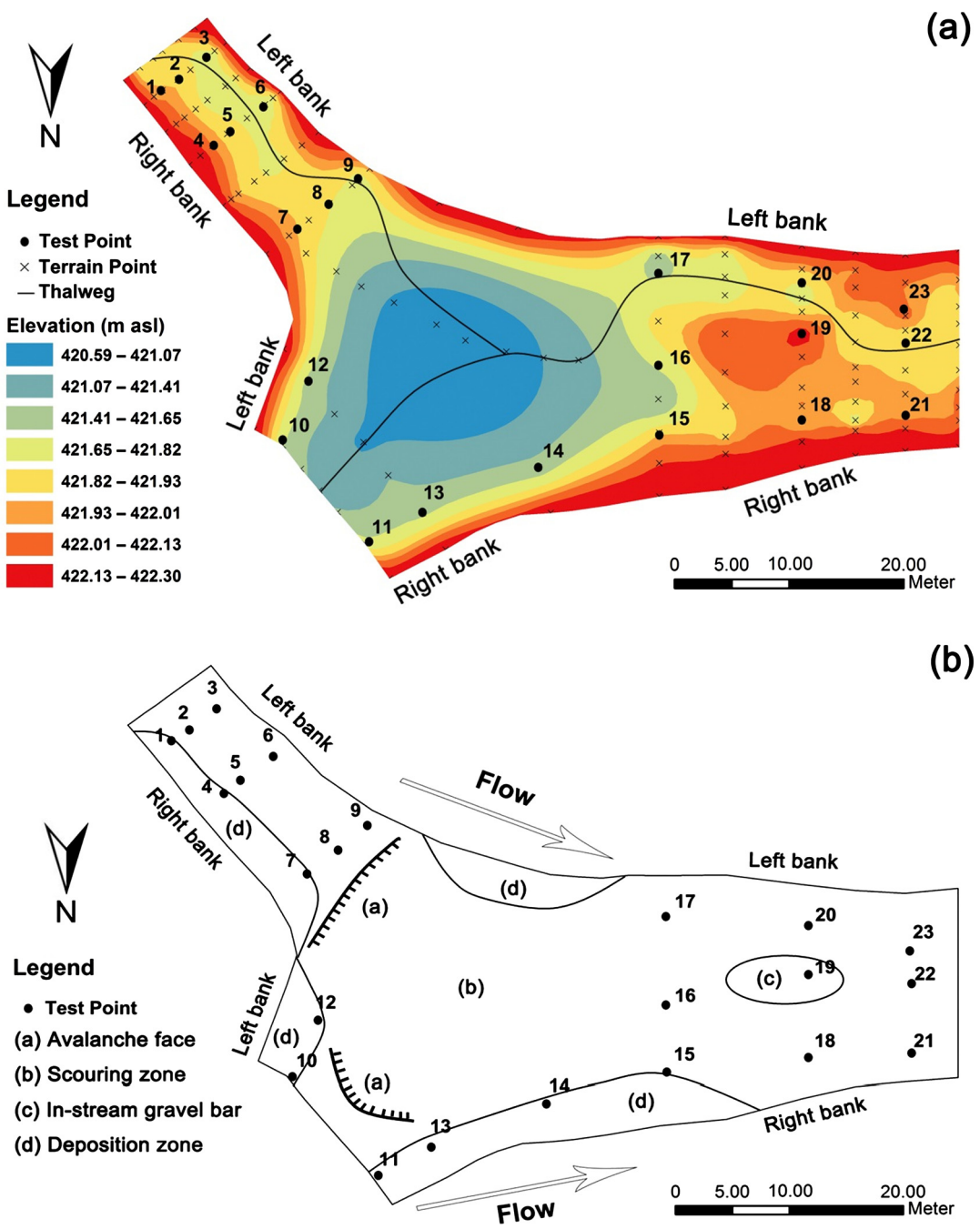

Fig. 2. (a) Streambed elevations above sea level and (b) characteristics of the riverbed morphology.

Table 2
Sediment particle size distributions at the river confluence (including M, T, and PM) during the test period.

Parameter		M			T			PM		
		R[a]	C[a]	L[a]	R[a]	C[a]	L[a]	R[a]	C[a]	L[a]
Cumulative weight[b] (%)	< 0.075 mm (silt/clay)	19.56	–[d]	15.46	7.44	2.07	0.53	5.18	1.03	4.56
	> 2 mm (gravel)	5.00	–[d]	10.16	19.36	29.37	30.86	12.30	20.41	11.13
d_{50}[c] (mm)		0.29	–[d]	0.18	1.26	0.80	0.59	0.39	0.84	0.59

[a] R, C, and L indicate the right bank, center, and left bank of the river, respectively, in the flow direction.
[b] Indicates the average cumulative percentage of the sediment grain size by weight.
[c] Indicates the average median grain size of the streambed sediments at the test site.
[d] Indicates that no data were obtained due to the water depth in the channel center upstream of the confluence (M).

Table 3
Main hydraulic parameters at the river confluence between the JR and HR during the test period.

Characteristic parameters	M	T	PM
Mean flow velocity (m/s)	2.04	1.48	1.03
Maximum flow velocity (m/s)	2.31	1.93	1.36
Width (m)	15.1–19.41	7.8–10.0	14.8–22.2
Mean width	17.28	8.52	17.42
Discharge (m^3/s)	13.52	6.17	19.69
Discharge ratio (T/M)	0.45		
Flow momentum ratio, M[a]	0.33		

[a] $M = (\rho Q_T V_T)/(\rho Q_M V_M)$, where ρ = water density (kg/m^3), Q = total discharge (m^3/s), and V = cross section averaged velocity (m/s).

dynamics, and the central scour zone was formed by the erosional stress of the downward flow. A shear layer (the imaginary line in Fig. 3) was observed in the middle of the helicoidal cells, which also formed by the confluence of the two flows. The location of the shear layer was also determined by the planform of the river confluence and flow momentum ratio. The Y-shaped confluence and the lesser flow momentum ratio (M < 0.5) resulted in the shear layer in the area south central of the junction. The formation of flow stagnation zones in the lee of each avalanche face also induced the occurrence of deposition zones in the same location. Meanwhile, in the lee of the helicoidal flow cell zone, the flow separation zone was observed with the river water that flows to both sides of the PM channel entrance (Leite Ribeiro et al., 2012). A flow recovery zone is located in the M channel near the third cross section by the flow direction (Fig. 3).

4.3. Patterns and magnitudes of hyporheic water exchange

The temperature data beneath the sediment-water interface were obtained during the test period. The patterns and magnitudes of the hyporheic water exchange were determined by the one-dimensional heat transport model based on the estimated temperature distributions of each test point. The values of the hyporheic water exchange ranged from −243.91 mm/d to 14.71 mm/d, and the negative and positive values indicated upwelling and downwelling at the test point, respectively. Additionally, the magnitudes of the water exchange at these 20 test points were negative, which indicated that the upwelling flow dominated the test area during the test period. Therefore, downwelling was observed at test points 1 T and 2 T of the T channel and test point 14PM (Fig. 4). For the magnitudes of the hyporheic water exchange, large flux variabilities were measured in the river confluence (Fig. 5). The range of the hyporheic water exchange fluxes for the entire river confluence was from −315.83 mm/d to 14.71 mm/d. The largest variability of the water exchange fluxes was observed in the PM channel where more complex riverbed morphology occurred (from −10.74 mm/d to −315.83 mm/d), and the minimum variability was observed in the M channel (from −2.81 mm/d to 14.71 mm/d) (Fig. 5). The mean of the hyporheic water exchange magnitudes of the PM channel, M channel and T channel were −109.36 mm/d, −23.18 mm/d and −82.91 mm/d, respectively (Fig. 5). The upwelling and downwelling occurred simultaneously in the T and M channels, and only upwelling occurred in the PM channel. The magnitudes of the three downwelling test points were generally lower, which indicated that the downwelling process was relatively weak compared to the upwelling in the test area. A strong upwelling zone was observed in the left bank of the T channel, and the center and left banks of the PM channel (the mean values of the upwelling fluxes in the three zones were −178.14 mm/d, −148.33 mm/d and −122.55 mm/d, respectively) (Fig. 6). The hyporheic water exchange process was weak, whether upwelling and downwelling at the right or left bank within the M channel, although the data of the hyporheic water exchange flux were not obtained due to the limitation of the large water depth and streambed materials in the center of the M channel. Notably, the largest absolute upwelling flux value was observed at test point 19PM (-315.83 mm/d), where a large gravel bar was formed (Fig. 2), and stronger downwelling occurred at test point 14PM (Fig. 6).

5. Discussion

The patterns and magnitudes of hyporheic water exchange are significantly impacted by the topography of the riverbed (Kasahara and Wondzell, 2003). The primary pattern of the hyporheic water exchange is determined by the groundwater and surface water levels at the regional scale. The groundwater and surface water level data in the test area from 9 to 13 July 2016 indicated that the groundwater level

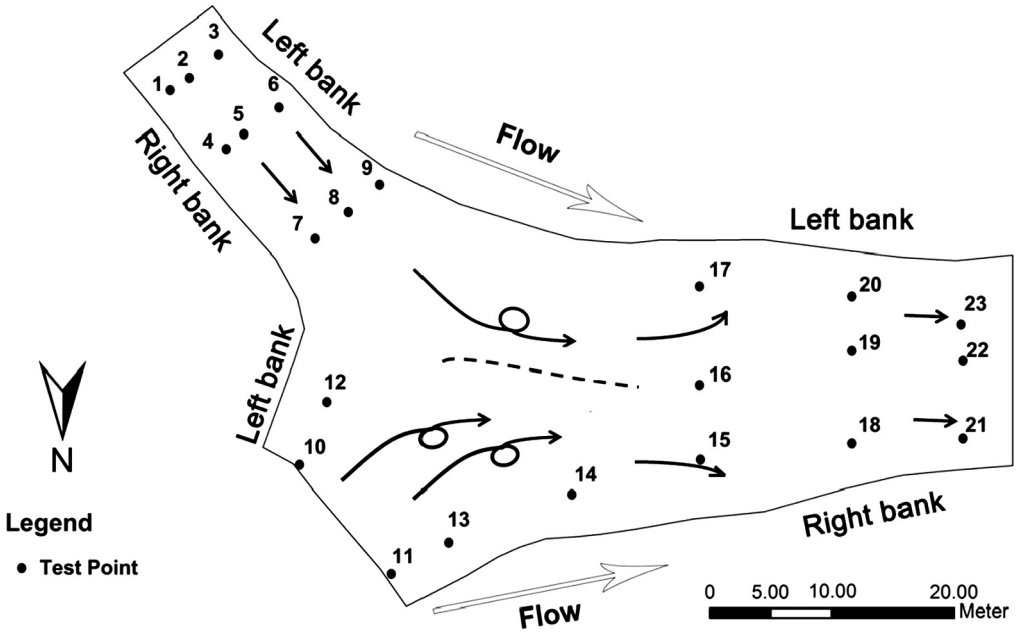

Fig. 3. Characteristics of the flow dynamics within the river confluence. The helicoidal arrows, curved arrows, and straight arrows indicate helicoidal flow, deflecting flow and straight flow, respectively.

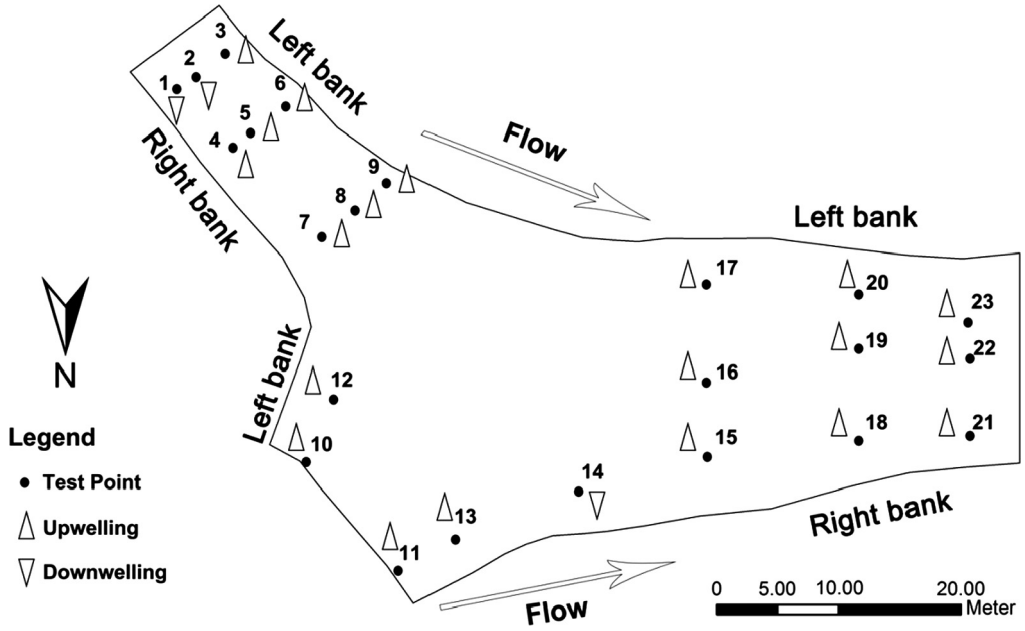

Fig. 4. Patterns of the hyporheic water exchange at each test point.

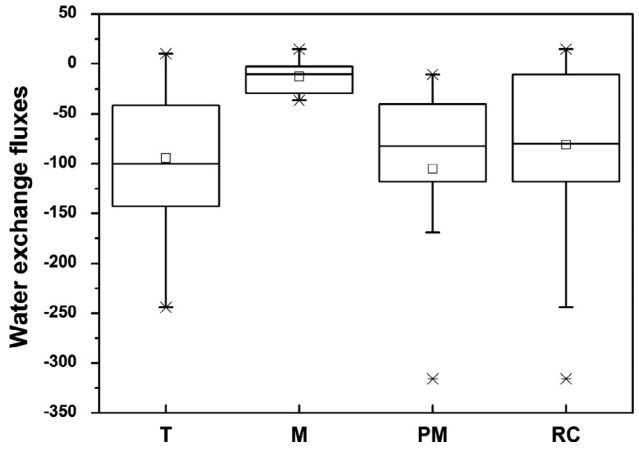

Fig. 5. Box plots of hyporheic water exchange fluxes at each test point during the test period. RC = river confluence; M = main channel; PM = postconfluence main channel; and T = tributary channel.

stabilized at approximately 422.90 m and the surface water level was approximately 422.30 m during the entire test period. In locations where the groundwater level was higher than the surface water level, groundwater discharge into the surface water through the hyporheic zone on a regional scale commonly occurred (Wang et al., 2018). Regionally, the upwelling hyporheic water exchange may be induced by groundwater discharged into the river (Hyun et al., 2011). However, different patterns were caused by the complicated topography of riverbed areas at the meter scale (Song et al., 2016; Zhang et al., 2016). In the field study, the downwelling process was observed at test point 1 T and test point 2 T. Notably, based on the investigation of the elevation, a deflection of the thalweg was found in the zone nearby test point 1 T and test point 2 T (Fig. 2). Portions of the surface water enter the hyporheic zone when occurs flow through the zone due to the barrier of the higher sediment, furthermore, the weak downwelling resulted from this hyporheic flow (Harvey and Bencala, 1993; Kasahara and Wondzell, 2003). The downwelling was also observed at test point 14PM, which was located in the zone of the helicoidal flow cells. The downwelling flow in the zone of the helicoidal flow cells may be caused by the occurrence and impact of the two flows (Szupiany et al., 2009). According to the analysis of Best (1988), in the zone of the helicoidal flow cells, the direction of the flow translates downward due to the encounter and impact of the two flows. Furthermore, the downward flow caused the surface water to enter the hyporheic zone and form downwelling. Notably, the stronger momentum of the flow in the M channel caused by a large discharge and flow velocity may have resulted in a stronger downwelling process at test point 14PM than the downwelling at test point 1 and test point 2. Meanwhile, Cardenas et al.

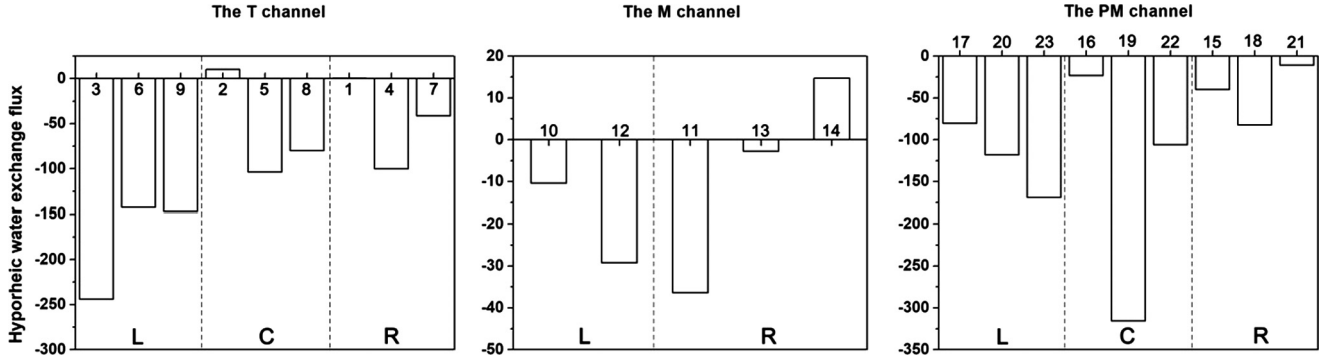

Fig. 6. Bar graphs of hyporheic water exchange fluxes at each test point during the test period. L = left bank of channel; C = center of channel; R = right bank of channel.

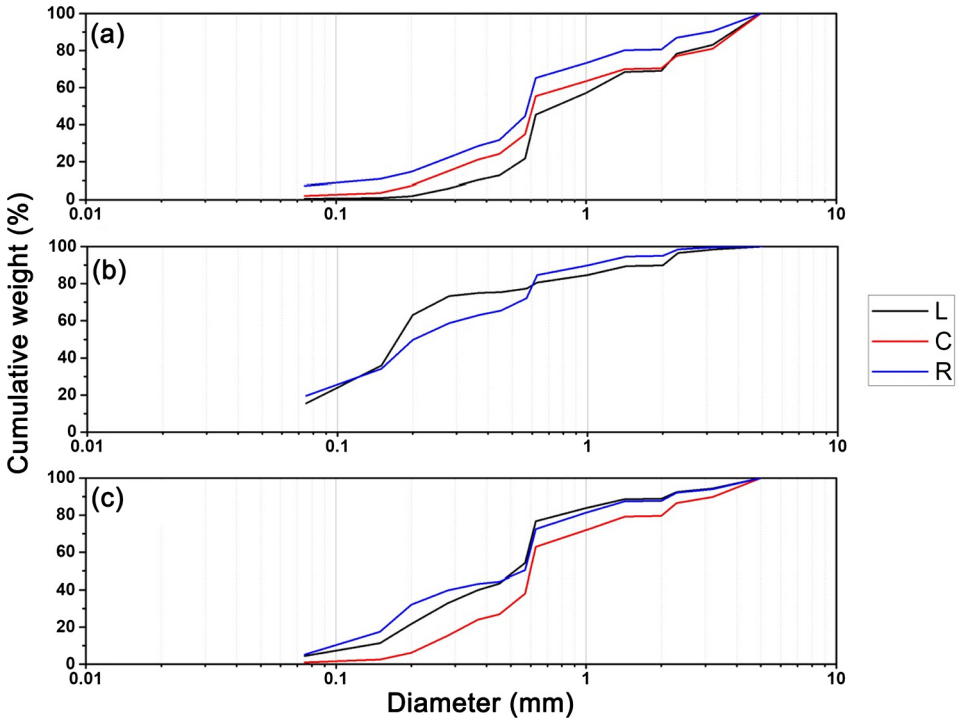

Fig. 7. Average grain size distributions of the streambed sediment along the right bank (R), the center (C), and the left bank (L) of the rivers in different channels during the test period, including the (a) tributary channel segment, (b) main channel segment, and (c) PM channel.

(2004) suggested that the cross-stream pressure gradients along meanders also increased in the downwelling flux in the confluent meander bend channel. Furthermore, the different patterns may cause the adsorption and release of contaminants within the hyporheic zone (Briggs et al., 2014).

Previous studies suggested that sediment particle distributions caused by erosional and depositional processes controlled by the obtuse junction angle (115°) and lower momentum flux ratio ($M < 0.5$) of the river confluence have significant effects on the magnitudes of hyporheic water exchange whether upwelling and downwelling (Kenworthy and Rhoads, 1995; Song et al., 2016; Wang et al., 2018). However, large spatial variability of the sediment particle distributions was found in different zones of the three channels (Fig. 7). Notably, lesser upwelling fluxes were generally observed in the depositional zone determined by the riverbed morphological and general hydraulic characteristics as well as the sediment particle distributions (the depositional zone included test points 4 T, 7 T, 10 M, 12 M, 11 M, 13 M and 15PM, and with upwelling, the mean value of the upwelling fluxes was −37.18 mm/d). In the nearby zone of the thalweg (including test points 3 T, 5 T, 6 T, 9 T, 17PM, 19PM, 20PM, and 22PM), the upwelling fluxes were generally higher at these test points. In addition, the phenomena were closely linked to the sediment particle distributions of the test points. A favorable correlation between the absolute value of upwelling fluxes and the d50 of test points was found by Pearson bivariate correlation analysis ($r = 0.526$, $p = 0.017$), indicating the larger upwelling flux generally occurred at the test point with a large d50 value. In the field study, the d50 values have significant positive and negative correlations with the weight percentage of the gravel and clay at each test point ($r_1 = 0.715$, $p_1 = 0.000$; $r_2 = -0.463$, $p_2 = 0.026$). Song et al (2016) suggested that a large amount of clay and less gravel may result in lower vertical hydraulic conductivity, further hindering the hyporheic water exchange. The largest upwelling magnitude occurred at test point 19PM where a large gravel bar with larger sediment particle size formed, which enhanced the process of upwelling. In addition, according to the analysis of Zhou et al. (2013), surface water generally enters into to in-stream gravel bar at the front of the bar and discharges behind the bar. A portion of hyporheic flow may enhance the upwelling process at test point 19PM, which is behind the bar (Fox et al., 2018).

6. Conclusions

The topographic characteristics of the river confluence were evaluated during the test period, whereas the general hydraulic characteristics and sediment particle distributions affected by the topography were investigated in a field study. Additionally, the patterns and magnitudes of hyporheic water exchange were estimated by the one-dimensional heat transport modal at each test point.

Based on the flow dynamics and sediment particle distributions induced by the riverbed topography characteristics, a deposition zone was observed in the right bank of the T channel and on both sides of the M channel, and a large gravel bar formed in the zone near test point 19PM within the PM channel. Erosional zones generally occurred in the vicinity of the thalweg and the magnitude of hyporheic water exchange was significantly affected by the sediment particle distributions resulting from erosional and depositional processes. Upwelling dominated the test area, and a weak downwelling process occurred at three of 23 total test points. The predominant pattern of water exchange was determined by the level of the surface water and groundwater at the regional scale. However, a complicated riverbed topography may cause different water exchange patterns at the meter scale, such as the deflection of the thalweg and helicoidal flow in the center of confluence, which cause downwelling and groundwater recharge by river water. Therefore, this study can provide a scientific reference for a clearer understanding of small-scale variability in hyporheic water exchange affected by riverbed morphology. The finding of the study could be useful to the management of water quantity and quality in this area and other similar areas. Nonetheless, potential limitations may cause by the short time testing. In further study, long-term testing will be encouraged to improve understanding of hyporheic water exchange processes and dynamics.

Declaration of interest

None.

Acknowledgements

This study was jointly supported by the National Natural Science Foundation of China (Grant Nos. 51679200 and 51379175), Hundred Talents Project of the Chinese Academy of Sciences (Grant No. A315021406) and Program for Key Science and Technology Innovation Team in Shaanxi Province (Grant No. 2014KCT-27). Especially, we are grateful to the editor and three anonymous reviewers who provided numerous comments and suggestions that improved the manuscript.

References

Anderson, M.P., 2005. Heat as a ground water tracer. Groundwater 43, 951–968. https://doi.org/10.1111/j.1745-6584.2005.00052.x.

Anibas, C., Fleckenstein, J.H., Volze, N., Buis, K., Verhoeven, R., Meire, P., Batelaan, O., 2009. Transient or steady-state? Using vertical temperature profiles to quantify groundwater–surface water exchange. Hydrological Process. 23, 2165–2177. https://doi.org/10.1002/hyp.7289.

Arriaga, M.A., Leap, D.I., 2006. Using solver to determine vertical groundwater velocities by temperature variations, Purdue University, Indiana, USA. Hydrogeol. J. 14, 253–263. https://doi.org/10.1007/s10040-004-0381-x.

Best, J.L., 1986. The morphology of river channel confluences. Prog. Phys. Geogr. 10 (2), 157–174. https://doi.org/10.1177/030913338601000201.

Best, J.L., 1988. Sediment transport and bed morphology at river channel confluences. Sedimentology 35, 481–498. https://doi.org/10.1111/j.1365-3091.1988.tb00999.x.

Best, J.L., Rhoads, B.L., 2008. Sediment Transport, Bed Morphology and the Sedimentology of River Channel Confluences//River Confluences, Tributaries and the Fluvial Network. John Wiley & Sons, Ltd 10.1002/9780470760383.ch4.

Boano, F., Camporeale, C., Revelli, R., Ridolfi, L., 2006. Sinuosity-driven hyporheic exchange in meandering rivers. Geophys. Res. Lett. 33. https://doi.org/10.1029/2006GL027630.

Boulton, A.J., Findlay, S., Marmonier, P., Stanley, E.H., Valett, H.M., 1998. The functional significance of the hyporheic zone in streams and rivers. Annu. Rev. Ecol. Syst. 29, 59–81.

Boyle, J.M., Saleem, Z.A., 1979. Determination of recharge rates using temperature-depth profiles in wells. Water Resour. Res. 15, 1616–1622. https://doi.org/10.1029/WR015i006p01616.

Bredehoeft, J., Papaopulos, I., 1965. Rates of vertical groundwater movement estimated from the earth's thermal profile. Water Resour. Res. 1, 325–328.

Briggs, M.A., Lautz, L.K., Hare, D.K., 2014. Residence time control on hot moments of net nitrate production and uptake in the hyporheic zone. Hydrol. Process. 28, 3741–3751. https://doi.org/10.1002/hyp.9921.

Brunke, M., Gonser, T., 1997. The ecological significance of exchange processes between rivers and groundwater. Freshw. Biol. 37 (1), 1–33. https://doi.org/10.1046/j.1365-2427.1997.00143.x.

Cardenas, M.B., Wilson, J.L., Zlotnik, V.A., 2004. Impact of heterogeneity, bed forms, and stream curvature on subchannel hyporheic exchange. Water Resour. Res. 40. https://doi.org/10.1029/2004WR003008.

Chen, C., Ahmad, S., Kalra, A., Xu, Z.X., 2017a. A dynamic model for exploring water-resource management scenarios in an inland arid area: Shanshan County, Northwestern China. J. Mountain Sci. 14, 1039–1057. https://doi.org/10.1007/s11629-016-4210-1.

Chen, C., Kalra, A., Ahmad, S., 2018. Hydrologic responses to climate change using downscaled gcm data on a watershed scale. J. Water Climate Change jwc2018147. https://doi.org/10.2166/wcc.2018.147.

Chen, Z., Zhang, R.R., Han, S.S., 2017b. An enhanced environmental multimedia modelling system (FEMMS): Part I–development and model verification. Environ. Eng. Manage. J. 16, 1009–1020.

Cranswick, R.H., Cook, P.G., Lamontagne, S., 2014. Hyporheic zone exchange fluxes and residence times inferred from riverbed temperature and radon data. J. Hydrol. 519, 1870–1881. https://doi.org/10.1016/j.jhydrol.2014.09.059.

Engelhardt, I., Piepenbrink, M., Trauth, N., Stadler, S., Kludt, C., Schulz, M., Schüth, C., Ternes, T.A., 2011. Comparison of tracer methods to quantify hydrodynamic exchange within the hyporheic zone. J. Hydrol. (Amsterdam) 400 (1–2), 255–266. https://doi.org/10.1016/j. jhydrol.2011. 01.033.

Fischer, H., Kloep, F., Wilzcek, S., Pusch, M.T., 2005. A River's Liver – microbial Processes within the Hyporheic Zone of a Large Lowland River. Biogeochemistry 76, 349–371. https://doi.org/10.1007/s10533-005-6896-y.

Fox, A., Packman, A.I., Boano, F., Phillips, C.B., Arnon, S., 2018. Interactions between suspended kaolinite deposition and hyporheic exchange flux under losing and gaining flow conditions. Geophys. Res. Lett. 45, 4077–4085. https://doi.org/10.1029/2018GL077951.

Guo, W.Q., Song, J.X., Liu, Q., Zhang, G.T., Wang, W.Z., Tang, B., Dou, X.Y., 2018. Influence of hyporheic water exchange on quality of sediment pore water for the Juehe River in winter. Acta Scientiae Circumstantiae 38 (5), 1957–1967. https://doi.org/10.13671/j.hjkxxb.2018.0014.

Harvey, J.W., Bencala, K.E., 1993. The Effect of streambed topography on surface-subsurface water exchange in mountain catchments. Water Resour. Res. 29, 89–98. https://doi.org/10.1029/92WR01960.

Hatch, C.E., Fisher, A.T., Revenaugh, J.S., Constantz, J., Ruehl, C., 2006. Quantifying surface water–groundwater interactions using time series analysis of streambed thermal records: method development. Water Resour. Res. 42. https://doi.org/10.1029/2005WR004787.

Hill, A.R., Labadia, C.F., Sanmugadas, K., 1998. Hyporheic zone hydrology and nitrogen dynamics in relation to the streambed topography of a N-rich stream. Biogeochemistry 42, 285–310. https://doi.org/10.1023/A:1005932528748.

Hyun, Y., Kim, H., Lee, S.-S., Lee, K.-K., 2011. Characterizing streambed water fluxes using temperature and head data on multiple spatial scales in Munsan stream, South Korea. J. Hydrol. 402, 377–387. https://doi.org/10.1016/j.jhydrol.2011.03.032.

Jones, J.B., Holmes, R.M., 1996. Surface-subsurface interactions in stream ecosystems. Trends Ecol. Evol. 11, 239–242. https://doi.org/10.1016/0169-5347(96)10013-6.

Kalbus, E., Schmidt, C., Bayer-Raich, M., Leschik, S., Reinstorf, F., Balcke, G.U., Schirmer, M., 2007. New methodology to investigate potential contaminant mass fluxes at the stream–aquifer interface by combining integral pumping tests and streambed temperatures. Environ. Pollut. 148 (3). https://doi.org/10.1016/j.envpol.2007.01.042.

Kasahara, T., Wondzell, S.M., 2003. Geomorphic controls on hyporheic exchange flow in mountain streams. Water Resourc. Res. 39. https://doi.org/10.1029/2002WR001386.

Kenworthy, S.T., Rhoads, B.L., 1995. Hydrologic control of spatial patterns of suspended sediment concentration at a stream confluence. J. Hydrol. 168, 251–263. https://doi.org/10.1016/0022-1694(94)02644-Q.

Krause, S., Hannah, D.M., Fleckenstein, J.H., 2009. Hyporheic hydrology: interactions at the groundwater-surface water interface. Hydrol. Process. 23, 2103–2107. https://doi.org/10.1002/hyp.7366.

Leite Ribeiro, M., Blanckaert, K., Roy, A.G., Schleiss, A.J., 2012. Flow and sediment dynamics in channel confluences. J. Geophys. Res. Earth Surf. 117. https://doi.org/10.1029/2011JF002171.

Liu, Q., Song, J.X., Zhang, G.T., Wang, W.Z., Guo, W.Q., Tang, B., Kong, F.H., Huo, A.D., 2017. Effect of hyporheic water fluxes and sediment grain size on the concentration and diffusive flux of heavy metals in the streambed. Int. J. Environ. Res. Public Health 14 (1020). https://doi.org/10.3390/ijerph14091020.

Shope, C.L., Constantz, J.E., Cooper, C.A., Reeves, D.M., Pohll, G., McKay, W.A., 2012. Influence of a large fluvial island, streambed, and stream bank on surface water-groundwater fluxes and water table dynamics. Water Resour. Res. 48. https://doi.org/10.1029/2011WR011564.

Song, J., Cheng, D., Li, Q., He, X., Long, Y., Zhang, B., 2015. An evaluation of river health for the Weihe River in Shaanxi Province, China. Adv. Meteorol. 2015, 13. https://doi.org/10.1155/2015/476020.

Song, J., Jiang, W., Xu, S., Zhang, G., Wang, L., Wen, M., Zhang, B., Wang, Y., Long, Y., 2016. Heterogeneity of hydraulic conductivity and Darcian flux in the submerged streambed and adjacent exposed stream bank of the Beiluo River, northwest China. Hydrogeol. J. 24, 2049–2062. https://doi.org/10.1007/s10040-016-1449-0.

Stallman, R., 1965. Steady one-dimensional fluid flow in a semi-infinite porous medium with sinusoidal surface temperature. J. Geophys. Res. 70, 2821–2827.

Stonedahl, S.H., Harvey, J.W., Packman, A.I., 2013. Interactions between hyporheic flow produced by stream meanders, bars, and dunes. Water Resour. Res. 49, 5450–5461. https://doi.org/10.1002/wrcr.20400.

Storey, R.G., Williams, D.D., Fulthorpe, R.R., 2004. Nitrogen processing in the hyporheic zone of a pastoral stream. Biogeochemistry 69, 285–313. https://doi.org/10.1023/B:BIOG.0000031049.95805.ec.

Szupiany, R.N., Amsler, M.L., Parsons, D.R., Best, J.L., 2009. Morphology, flow structure, and suspended bed sediment transport at two large braid-bar confluences. Water Resour. Res. 45. https://doi.org/10.1029/2008WR007428.

Wang, T., Zlotnik, V.A., Wedin, D., Wally, K.D., 2008. Spatial trends in saturated hydraulic conductivity of vegetated dunes in the Nebraska Sand Hills: effects of depth and topography. J. Hydrol. 349, 88–97. https://doi.org/10.1016/j.jhydrol.2007.10.027.

Wang, P., Yu, J., Zhang, Y., Liu, C., 2013. Groundwater recharge and hydrogeochemical evolution in the Ejina Basin, northwest China. J. Hydrol. 476, 72–86. https://doi.org/10.1016/j.jhydrol.2012.10.049.

Wang, W., Song, J., Zhang, G., Liu, Q., Guo, W., Tang, B., Cheng, D., Zhang, Y., 2018. The influence of hyporheic upwelling fluxes on inorganic nitrogen concentrations in the pore water of the Weihe River. Ecol. Eng. 112, 105–115. https://doi.org/10.1016/j.ecoleng.2017.12.012.

Wei, S., Song, J., Khan, N.I., 2011. Simulating and predicting river discharge time series using a wavelet-neural network hybrid modelling approach. Hydrol. Process. 26, 281–296. https://doi.org/10.1002/hyp.8227.

Wondzell, S.M., Swanson, F.J., 1999. Floods, channel change, and the hyporheic zone. Water Resour. Res. 35, 555–567. https://doi.org/10.1029/1998WR900047.

Yang, L., Song, X., Zhang, Y., Han, D., Zhang, B., Long, D., 2012. Characterizing interactions between surface water and groundwater in the Jialu River basin using major ion chemistry and stable isotopes. Hydrol. Earth Syst. Sci. 9, 5955–5981. https://doi.org/10.5194/hess-16-4265-2012.

Zarnetske, J.P., Roy, H., Wondzell, S.M., Bokil, V.A., 2012. Coupled transport and reaction kinetics control the nitrate source-sink function of hyporheic zones. Water Resour. Res. 48, 11508. https://doi.org/10.1029/2012WR011894.

Zhang, G., Song, J., Wen, M., Zhang, J., Jiang, W., Wang, L., Kong, F., Wang, Y., 2016. Effect of bank curvatures on hyporheic water exchange at meter scale. Hydrol. Res. 48, 355–369. https://doi.org/10.2166/nh.2016.046.

Zhang, J., Zhang, Y., Song, J., Cheng, L., 2017. Evaluating relative merits of four baseflow separation methods in Eastern Australia. J. Hydrol. 549, 252–263. https://doi.org/10.1016/j.jhydrol.2017.04.004.

Zhi, J.H., Ding, A.Z., Cheng, L.R., Zhang, S.R., Zhao, X., 2013. Nitrogen pollution

characteristics and genetic analysis of fenghe river and its tributaries. Appl. Mech. Mater. 316–317, 227–230. https://doi.org/10.4028/www.scientific.net/AMM.316-317.227.
Zhou, Y., Ritzi, R.W., Soltanian, M.R., Dominic, D.F., 2013. The Influence of Streambed Heterogeneity on Hyporheic Flow in Gravelly Rivers. Groundwater 52, 206–216. https://doi.org/10.1111/gwat.12048.
Zhu, T., Fu, D., Jenkinson, B., Jafvert, C.T., 2015. Calibration and application of an automated seepage meter for monitoring water flow across the sediment-water interface. Environ. Monit. Assess. 187, 171. https://doi.org/10.1007/s10661-015-4388-7.